Band-Target Entropy Minimization (BTEM): An Advanced Method for Recovering Unknown Pure Component Spectra. Application to the FTIR Spectra of Unstable Organometallic Mixtures

Wee Chew, Effendi Widjaja, and Marc Garland*

Department of Chemical and Environmental Engineering, 4 Engineering Drive 4, National University of Singapore, Singapore 119260

Received October 5, 2001

A newly developed band-target entropy minimization (BTEM) algorithm was tested on experimental FTIR data of $Rh_4(CO)_{12}/Rh_6(CO)_{16}$ mixtures in order to recover the pure component spectra of the constituent complexes. Bands in the nonoverlapping bridging carbonyl region as well as bands in the highly overlapping terminal carbonyl region were targeted for retention. The bands are identified in the vector-space decomposition of the observations, a crucial first step in untangling the superposition of the pure component spectra. In both cases, the targeted band was retained, and exceptionally accurate whole spectral estimates of $Rh_4(CO)_{12}$ and $Rh_6(CO)_{16}$ were obtained. Due to the constructs used in BTEM, enhanced signal-to-noise characteristics result, and spectral nonlinearities arising from changing band positions and changing band shapes are essentially eliminated. For the experimentalist, the utility of BTEM arises from its direct one-spectrum-at-a-time spectral reconstruction approach—which is guided by the choice of the targeted region. As such, BTEM appears particularly applicable to spectroscopy possessing highly localized features: i.e., FTIR, Raman, etc. The BTEM algorithm is so useful that the spectral pattern from the minute presence of suspended particles of $Rh_6(CO)_{16}$ could be reconstructed. Indeed, the integrated absorbance of $Rh_4(CO)_{12}$, $Rh_6(CO)_{16}$, and $Rh_6(CO)_{16}$ solids account for only ca. 0.3, 0.09, and 0.04% of the experimental observations. The new BTEM algorithm was compared to other algorithms such as SIMPLISMA, IPCA, and OPA-ALS. The latter either fail with the present data set or are unable to produce reconstructed spectra of similar quality to BTEM. *This new algorithm holds considerable promise for the analysis of in-situ spectroscopic reaction data such as those arising in complex organometallic and organic syntheses*, where absolutely no *a priori* information about the constituents/intermediates is available.

Introduction

In a wide variety of problems occurring in the chemical sciences, pure component spectra are often needed. However, the experimentalist frequently encounters impure samples that resist further separation and purification. Simple examples include (1) many organometallic species that are acutely sensitive to trace moisture and oxygen or light or are otherwise thermally unstable and (2) organometallic species that are kinetically labile and easily interconvert. Even more challenging is the interpretation of the in-situ spectroscopic data from organic syntheses, particularly homogeneous catalytic syntheses, where FTIR or NMR measurements are performed and most if not all of the species are unknown.[1,2] In addition, the total absorbance due to the transient species will be very small, and "pure" samples of the such intermediates are impossible to obtain. In all of the above examples, a method for recovering the pure component spectra, one that is more robust and reliable than SIMPLISMA,[3] IPCA,[4] and OPA-ALS,[5] would be very useful.[6]

In this contribution, a new and powerful method for spectral reconstruction called band-target entropy minimization (BTEM) is introduced. The algorithm targets an individual feature from a vector-space decomposition

* To whom correspondence should be sent. E-mail: chemvg@nus.edu.sg.

(1) For a general introduction to in situ monitoring of organic syntheses: (a) Moser, W. R. In *Homogeneous Transition Metal Catalyzed Reactions: Developed from a Symposium*; Moser, W. R., Slocum, D. W., Eds.; American Chemical Society: Washington, D.C., 1992; p 3. (b) Whyman, R. *Ibid*., p 19. (c) Roe, D. C. *Ibid*., p 33.

(2) Specific examples from the well-known rhodium-catalyzed hydroformylation reaction include: (a) Garland, M.; Bor, G. *Inorg. Chem.* **1989**, *28*, 410. (b) Garland, M.; Pino, P. *Organometallics* **1991**, *10*, 1693. (c) Garland, M. *Organometallics* **1993**, *12*, 535. (d) Fyhr, C.; Garland, M. *Organometallics* **1993**, *12*, 1753. (e) Feng, J.; Garland, M. *Organometallics* **1999**, *18*, 417. (f) Liu, G.; Volken, R.; Garland, M. *Organometallics* **1999**, *18*, 3429. (g) Brown, J. M.; Kent, A. G. *J. Chem. Soc., Perkin Trans. 2* **1987**, 1597. (h) Brown, J. M.; Canning, L. R.; Kent, A. G.; Sidebottom, P. J. *J. Chem. Soc., Chem. Commun.* **1982**, 721. (i) Brown, J. M.; Kent, A. G. *J. Chem. Soc., Chem. Commun.* **1982**, 723.

(3) (a) Windig, W.; Guilment, J. *Anal. Chem.* **1991**, *63*, 1425. (b) Windig, W. *Chemom. Intell. Lab. Syst.* **1997**, *36*, 3.

(4) Bu, D.; Brown, C. W. *Appl. Spectrosc.* **2000**, *54*, 1214.

(5) (a) Sanchez, F. C.; Toft, J.; Van den Bogaert, B.; Massart, D. L. *Anal. Chem.* **1996**, *68*, 79. (b) Frenich, A. G.; Galera, M. M.; Vidal, J. L. M.; Massart, D. L.; Torres-Lapasio, J. R.; De Braekeleer, K.; Wang, J.; Hopke, P. K. *Anal. Chim. Acta* **2000**, *411*, 145.

(6) The latter methods often assume the number of observable species present and the existence of a so-called "pure wavelength" for each species. Both conditions are particularly restrictive, especially when a large but unknown number of species are present and their pure component spectra are highly overlapping.

10.1021/om0108752 CCC: $22.00
Publication on Web 04/22/2002

of the observations and subsequently reconstructs the corresponding whole pure component spectrum. In the present contribution, we show the usefulness of the BTEM algorithm in recovering pure undistorted spectra of exceptionally high quality for both $Rh_4(CO)_{12}$ and $Rh_6(CO)_{16}$ from *mixture* FTIR data. These rhodium clusters are two of the most extensively studied and utilized organometallic complexes for organic synthesis.[7] The former is sensitive to moisture, oxygen, and light. It is also thermally unstable.[8] The more stable $Rh_6(CO)_{16}$ is formed readily from $Rh_4(CO)_{12}$, resulting in the ever-present $Rh_6(CO)_{16}$ species in $Rh_4(CO)_{12}$ samples. As such, the published "pure" spectra of $Rh_4(CO)_{12}$ vary considerably in the literature. The BTEM algorithm also produces spectra with reduced noise and eliminates spectral features due to suspended solids.

Background

Although pure component spectral reconstruction has an extensive history,[9] one of the more interesting but rarely used approaches involves entropy minimization. Sasaki, Minami, et al. used entropy minimization in order to search for the simplest patterns which span a set of infrared spectroscopic observations.[10] These patterns provided a rough first approximation of the "pure" component spectra of xylene, toluene, and benzene. Entropy minimization is particularly appealing because of its generality. As such, no *a priori* information is required concerning the type of number of observable species present, and the experimentalist does not need to presuppose any particular type of spectral characteristics: i.e., Lorentz, Gaussian, and Pearson distribution etc. Thus, the spirit of entropy minimization methods is essentially model free. It is well-known that entropy minimization is also closely associated with pattern recognition.[11]

Recently, we have reexamined some numerical aspects of the use of entropy minimization in spectral reconstruction. The main findings were that fourth-order entropy type functions can greatly assist in resolving highly overlapping bands from limited spectral measurements[12] and that weighted piecewise continuous spectral measurements can overcome the problem of spectral windows having significantly different variance. These improvements were applied to a set of dilute $Co_2(CO)_8/Co_4(CO)_{12}$ mixture spectra.[13] It is well-known that $Co_2(CO)_8$ rapidly decomposes in solution, and thus its true "pure" FTIR spectra are very difficult to obtain. A set of eight mixture absorbance spectra $\mathbf{A}_{8\times\nu}$, with a total of ν channels, was subjected to singular value decomposition to obtain the right singular vectors. From these, the first two basis vectors $\mathbf{V}^{\mathrm{T}}_{2\times\nu}$, corresponding to $s = 2$ species present, were rotated into 2 pure component spectral estimates $\hat{\mathbf{a}}_{2\times\nu}$ by premultiplying with the optimized transformation matrix $\mathbf{T}_{2\times2}$ obtained via an entropy minimization algorithm (see Computational Aspects section for similar entropy functions), according to eq 1. Since the transformation matrix has dimensions

$$\hat{\mathbf{a}}_{s\times\nu} = \mathbf{T}_{s\times s}\mathbf{V}^{\mathrm{T}}_{s\times\nu} \tag{1}$$

$s \times s$, this is a "square" problem. The resulting spectra provided very good estimates of $Co_2(CO)_8$ and $Co_4(CO)_{12}$.

Although this "square problem" can be generalized to cases in which $s > 2$, two serious problems still remain, namely (1) the computational effort is exponential in s and (2) it cannot deal with shifting band positions and changing band shapes. The problem of shifting band positions and changing band shapes is of course ubiquitous in chemical spectroscopy and is often encountered when two different solution spectra are subtracted in order to obtain only one component. Such nonlinearities are often manifested as a sigmoidal baseline distortion. Shifting band position and changing band shapes can arise due to changes in composition, temperature, or even pressure.[14]

Consider a system with s species. If shifting band positions and changing band shapes exist in a set of spectroscopic data array $\mathbf{A}_{k\times\nu}$, then $z > s$ orthogonal vectors are required to span the set of experimental observations. In the context of spectral reconstruction, this gives rise to a "nonsquare problem" (eq 2). Such a

$$\hat{\mathbf{a}}_{s\times\nu} = \mathbf{T}_{s\times z}\mathbf{V}^{\mathrm{T}}_{z\times\nu} \qquad z > s \tag{2}$$

projection of all z basis vectors onto a lower dimensional subset should effectively eliminate spectral distortion due to shifting band positions and changing band shapes. The resulting reconstructed pure component spectra represent a set of chemically meaningful averaged spectra.

For a data array containing spectral nonlinearities and a large number of species, it would be numerically difficult and time-consuming to obtain the spectral estimates according to eq 2, since the solution requires the determination of $s \times z$ elements in the transformation matrix. Therefore, instead of solving for s spectral estimates at once, an algorithm that produces estimates one at a time according to eq 3 would be very useful.

$$\hat{\mathbf{a}}_{1\times\nu} = \mathbf{T}_{1\times z}\mathbf{V}^{\mathrm{T}}_{z\times\nu} \qquad z > s \tag{3}$$

Accordingly, we have implemented a band-targeted use of eq 3 as the basis for the BTEM algorithm. A vector-space decomposition of the observations results in a crucial initial untangling of the pure component spectra. From this decomposition, the user can interactively choose an interesting spectral feature to retain. *The BTEM algorithm then forces the retention of this spectral feature and, at the same time, reconstructs the*

(7) (a) Dickson, R. S. *Homogeneous Catalysis with Compounds of Rhodium and Iridium*; Reidel: Dordrecht, The Netherlands, 1986. (b) van Leeuwen, P. W. N. M.; Claver, C. *Rhodium Catalyzed Hydroformylation*; Kluwer Academic: Boston, 2000.

(8) *Dictionary of Organometallic Compounds*; Hodgson, A., Ed.; Chapman and Hall: London; New York, 1984.

(9) (a) Lawton, W. H.; Sylvestre, E. A. *Technometrics* **1971**, *13*, 617. (b) Sylvestre, E. A.; Lawton, W. H.; Maggio, M. S. *Technometrics* **1973**, *45*, 353. (c) Ohta, N. *Anal. Chem.* **1973**, *45*, 553.

(10) (a) Sasaki, K.; Kawata, S.; Minami, S. *Appl. Opt.* **1983**, *22*, 3599. (b) Sasaki, K.; Kawata, S.; Minami, S. *Appl. Opt.* **1984**, *23*, 1955. (c) Kawata, S.; Komeda, H.; Sasaki, K.; Minami, S. *Appl. Spectrosc.* **1985**, *39*, 610.

(11) Watanabe, S. *Pattern Recognit.* **1981**, *13*, 381.

(12) Zeng, Y.; Garland, M. *Anal. Chim. Acta* **1998**, *359*, 303.

(13) Pan, Y.; Susithra, L.; Garland, M. *J. Chemometrics* **2000**, *14*, 63.

(14) (a) Nyquist, R. A. *Appl. Spectrosc.* **1986**, *40*, 79. (b) Nyquist, R. A.; Vhrzan, V.; Houck, J. *Appl. Spectrosc.* **1989**, *43*, 891. (c) Nyquist, R. A.; Putzig, C. L.; Yurga, L. *Appl. Spectrosc.* **1989**, *43*, 983. (d) Engberts, J. B. F. N.; Perjessy, A.; Blandamer, M. J. *J. Chem. Soc., Faraday Trans.* **1993**, *89*, 4199.

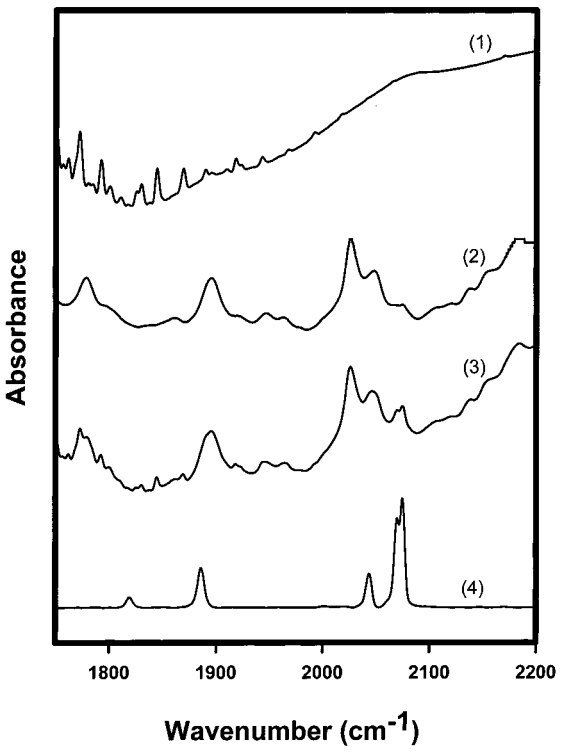

Figure 1. Preconditioning of $Rh_4(CO)_{12}/Rh_6(CO)_{16}$ mixture spectra: (1) background spectrum; (2) *n*-hexane solvent in CaF_2 cell spectrum; (3) raw $Rh_4(CO)_{12}/Rh_6(CO)_{16}$ mixture spectrum directly obtained from FTIR spectrophotometer; (4) preconditioned $Rh_4(CO)_{12}/Rh_6(CO)_{16}$ mixture spectrum.

entire associated function (pure component spectrum). As such, the algorithm is straightforward and goal-oriented.

Results

Preconditioned Spectra. Preconditioning of 10 experimental FTIR $Rh_4(CO)_{12}/Rh_6(CO)_{16}$ *mixture* spectra was performed as described in Computational Aspects. A sample result is provided by Figure 1, where background, the CaF_2 cell with *n*-hexane, a mixture spectrum, and a preconditioned spectrum are shown. These mixture spectra after preconditioning were consolidated into one preconditioned absorbance data matrix, $\mathbf{A}_{10\times2251}$, with 10 *mixture* spectra (rows) and 2251 channels of data (columns), shown in Figure 2. For subsequent discussion, it is useful to note the exceptionally small magnitude of the organometallic signals in Figures 1 and 2.

Singular Value Decomposition. The preconditioned data matrix $\mathbf{A}_{10\times2251}$ was subjected to singular value decomposition (SVD), yielding the orthonormal matrices $\mathbf{U}_{10\times10}$ and $\mathbf{V}^{\mathrm{T}}_{2251\times2251}$ and the singular matrix $\Sigma_{10\times2251}$, with its diagonal elements equal to singular values of $\mathbf{A}_{10\times2251}$.[15] The row vectors in the $\mathbf{V}^{\mathrm{T}}$ matrix are abstract orthogonal basis vectors that span the vector space for the pure component spectra contained in $\mathbf{A}_{10\times2251}$. Although a total of 2251 right singular vectors of $\mathbf{V}^{\mathrm{T}}$ were obtained, only the first 10 $\mathbf{V}^{\mathrm{T}}$ vectors are physically meaningful, as 10 mixture spectra are in the original data array $\mathbf{A}_{10\times2251}$. The first 5 $\mathbf{V}^{\mathrm{T}}$ vectors as well as the 10th $\mathbf{V}^{\mathrm{T}}$ vector are presented in Figure 3.

It is important to note that the right singular vectors in the $\mathbf{V}^{\mathrm{T}}$ matrix are ordered according to their contribution to the total variance of the observations. Therefore, the first few vectors are associated with real chemically important signals in the system and the remainder are associated primarily with the random instrumental and experimental noise. Accordingly, inspection of the first *four* right singular vectors strongly suggests the existence of chemically important spectral features.[16] Indeed, there are regions of localized signal intensity, and these correspond to the regions where absorbance from terminal and bridging metal−carbonyl vibrations can be expected. The remaining *six* vectors, i.e., the 5th through 10th right singular vectors, represent to a good first approximation only randomly distributed noise. Little if any localized signal intensity can be identified.

Pure Component Reconstruction Results via BTEM: Bridging Carbonyl Regions. The right singular vectors of the $\mathbf{V}^{\mathrm{T}}$ matrix were inspected for significant spectral features/extrema to be used as targets in the BTEM algorithm. From the first $\mathbf{V}^{\mathrm{T}}$ vector, two significant bands in the bridging carbonyl region (indicated by asterisks in Figure 3) were chosen for the reconstruction. These spectral features also appear in the second and third right singular vectors. The two targeted band regions were chosen as 1818−1820 and 1885−1887 cm^{-1}.[17]

It is worth repeating that in this *two* soluble organometallic species system, the spectral features of the bridging carbonyl are easily seen in the first *three* vectors, and spectral features of the terminal carbonyls are seen in the first *four* vectors. This is clear-cut irrefutable confirmation for the existence of spectral nonlinearities. In contrast, for a two-species system with stationary carbonyl signals, identically two vectors are sufficient for the basis.

Spectral reconstruction based with $z = 2$, 4, and 10 was performed. This resulted in the spectral reconstruction of $Rh_4(CO)_{12}$ and $Rh_6(CO)_{16}$. The results are shown in Figures 4 and 5. For comparison purposes, the first spectrum in each figure was obtained from experimental measurements of "pure" stock solutions of $Rh_4(CO)_{12}$ and $Rh_6(CO)_{16}$ after preconditioning.

In Figure 4, the "pure" stock solution of $Rh_4(CO)_{12}$ clearly shows the presence of trace contamination by $Rh_6(CO)_{16}$, as evidenced by the absorbance at 1818 cm^{-1}. The first spectral reconstruction with $z = 2$ resulted in a very good estimate of $Rh_4(CO)_{12}$, with little absorbance from $Rh_6(CO)_{16}$. The spectral estimate is very smooth, with an entropy value of 5.734. The second spectral reconstruction with $z = 4$ also resulted in a very good estimate of $Rh_4(CO)_{12}$. The spectrum is somewhat smoother, with an entropy value of 5.630. Finally, the last spectral reconstruction with $z = 10$ provided the best estimate of $Rh_4(CO)_{12}$, free from any detectable

(15) Scheick, J. T. *Linear Algebra with Applications*; McGraw-Hill: Singapore, 1997.

(16) As shown (*vide infra*), there are two soluble species present and one suspended solid spectrum. Since at least four vectors are needed to represent three species, serious spectral nonlinearities exist (non-stationary signals). Statistical tests for determining the rank of the spectroscopic data would conflict with the actual number of species present.

(17) *17.* $\alpha = 3.0$ and $\alpha = 5.0$ is used in eq 20 for the targeted regions 1885−1887 and 1818−1820 cm^{-1}, respectively.

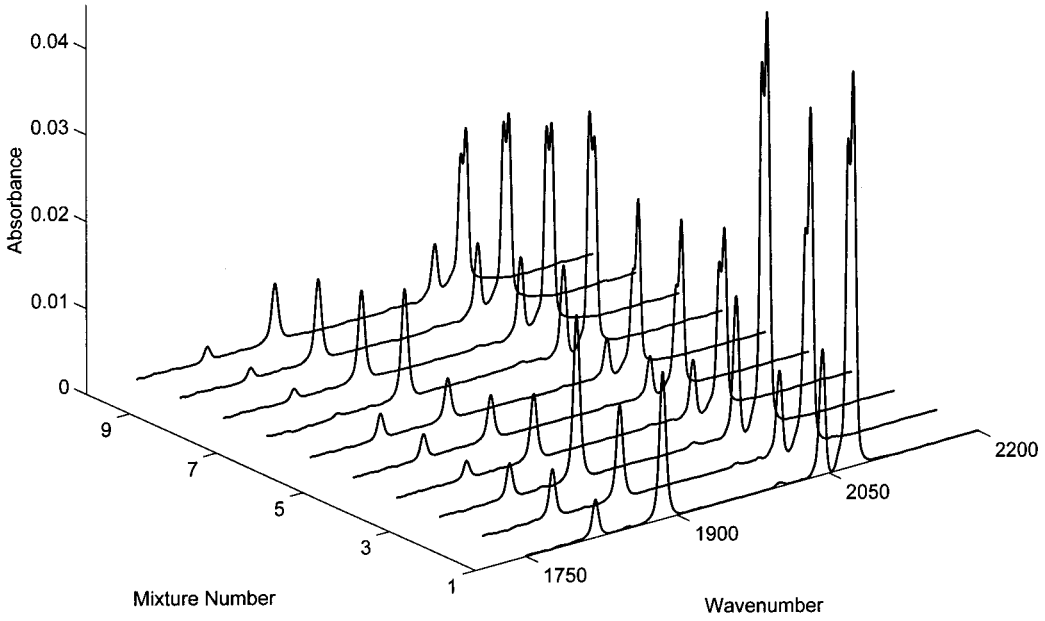

Figure 2. Consolidated preconditioned $Rh_4(CO)_{12}/Rh_6(CO)_{16}$ $\mathbf{A}_{10\times2251}$ absorbance data matrix.

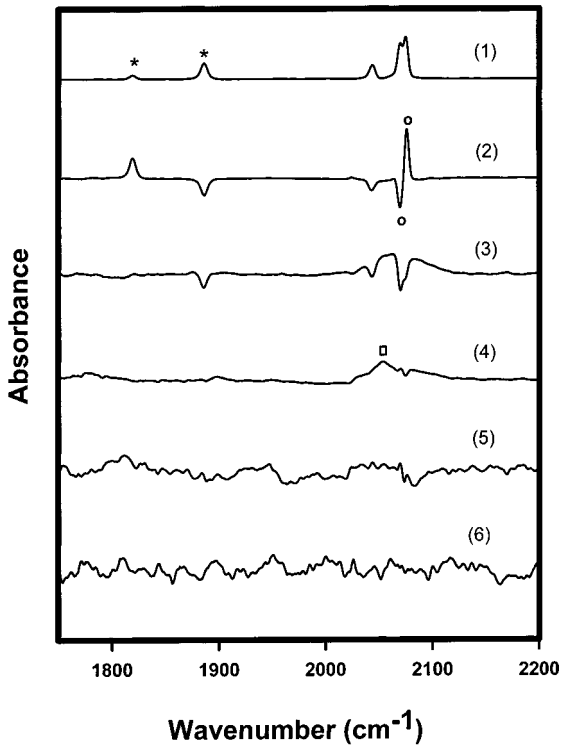

Figure 3. First five and tenth right singular vectors of $\mathbf{V}^T$ matrix: (1) first vector; (2) second vector; (3) third vector; (4) fourth vector; (5) fifth vector; (6) tenth vector.

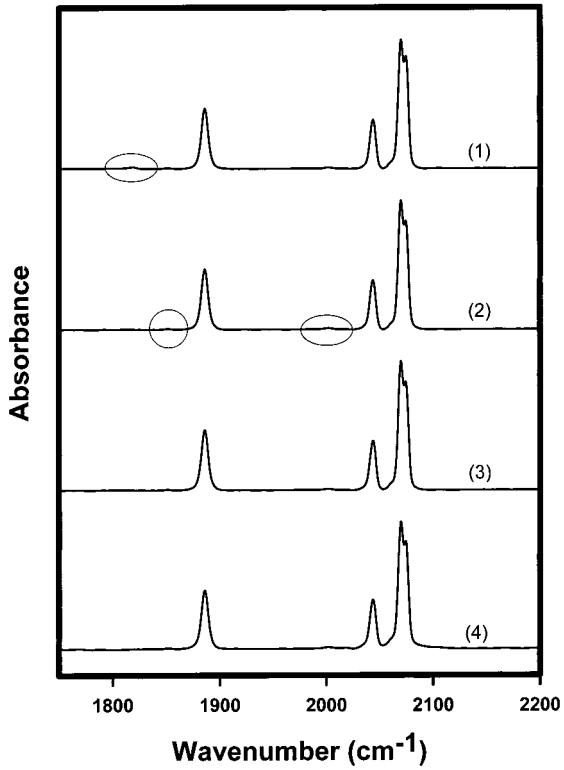

Figure 4. Experimental and estimated $Rh_4(CO)_{12}$ spectra via BTEM: (1) "pure" preconditioned spectrum from experiment, with circled region showing spectral contamination due to trace amounts of $Rh_6(CO)_{16}$; (2) estimated spectrum via BTEM with $z = 10$, with circled regions indicating ^{13}CO isotopomer peaks; (3) estimated spectrum via BTEM with $z = 4$; (4) estimated spectrum via BTEM with $z = 2$.

absorbance from $Rh_6(CO)_{16}$. The entropy value of this estimate was 5.623. Simpler and more refined spectra are progressively obtained. The estimates obtained from the BTEM algorithm are so smooth, and contain so little noise, that the absorbance from the 1.1% ^{13}CO isotopomers can be clearly identified at ca. 1851 and 2002 cm^{-1}.

This raises a new important point. Since the amount of ^{13}CO is not independently varied in these experiments, the pure component spectra of $Rh_4(\sigma\text{-}^{12}CO)_9(\mu\text{-}^{12}CO)_2(\mu\text{-}^{13}CO)$ and $Rh_4(\sigma\text{-}^{12}CO)_8(\sigma\text{-}^{13}CO)(\mu\text{-}^{12}CO)_3$ cannot be separately determined and therefore remain imbedded in the "pure component spectrum" of $Rh_4(CO)_{12}$. Likewise, if any other structural isomers of $Rh_4(CO)_{12}$ coexist simultaneously in solution, their spectra will remain imbedded in the "$Rh_4(CO)_{12}$ spectrum" unless some additional parameter such as pressure or

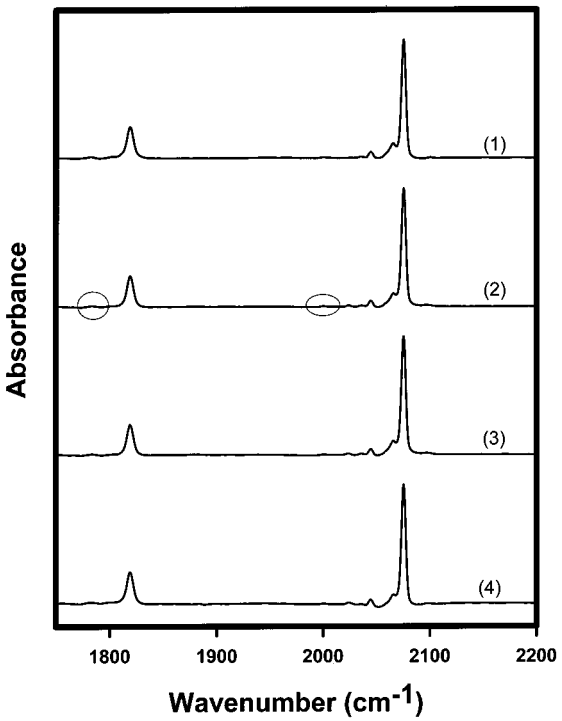

Figure 5. Experimental and estimated $Rh_6(CO)_{16}$ spectra via BTEM: (1) "pure" preconditioned spectrum from experiment; (2) estimated spectrum via BTEM with $z = 10$, with circled regions indicating ^{13}CO isotopomer peaks; (3) estimated spectrum via BTEM with $z = 4$; (4) estimated spectrum via BTEM with $z = 2$.

temperature is varied. Thus experimental design is a limiting factor for the recoverability of "pure component spectra".

In Figure 5, the "pure" stock solution of $Rh_6(CO)_{16}$ appears to be free of $Rh_4(CO)_{12}$. The first spectral reconstruction with $z = 2$ resulted in a very good estimate of $Rh_6(CO)_{16}$. The spectral estimate is very smooth, with an entropy value of 5.341. However, the spectral minimum at ca. 2052 cm^{-1} is slightly negative, due to the soft constraint used in the objective function (see Computational Aspects). The second spectral reconstruction with $z = 4$ also resulted in a very good estimate of $Rh_6(CO)_{16}$. The spectrum is somewhat smoother, with an entropy value of 5.327, and the minimum at ca. 2052 cm^{-1} is now nonnegative. Finally, the last spectral reconstruction with $z = 10$ provided the best estimate of $Rh_6(CO)_{16}$, with an entropy value of 5.299. Thus, simpler and more refined spectra are progressively obtained. Again, the BTEM algorithm produces spectra that have so little noise that the absorbance from the 1.1% ^{13}CO isotopomers can be seen at ca. 1784 and 2000 cm^{-1}. The comment made in the previous paragraph concerning recoverability of pure component spectra and isotomers for $Rh_4(CO)_{12}$ also holds for the present case of $Rh_6(CO)_{16}$.

It is quite instructive to consider the total integrated absorbance of $Rh_4(CO)_{12}$ and $Rh_6(CO)_{16}$ in the original experimental data. These numbers are very small and correspond to only ca. 0.3 and 0.09%, respectively.

Pure Component Reconstruction Results via BTEM: Terminal Carbonyl Regions. The previous section concentrated on the simple bridging carbonyl region because it provides a straightforward means of explaining the BTEM algorithm. However, the real utility of BTEM is found when complex highly overlapping spectra occur. Accordingly, the nontrivial terminal carbonyl region of the preconditioned data from 2050 to 2080 cm^{-1} is considered. Since the first four right singular vectors in Figure 3 show spectral features/extrema/inflections at ca. 2070 and 2075.5 cm^{-1}, which are particularly pronounced in the second vector (see circles), the regions 2069−2071 and 2075−2076 cm^{-1} were targeted.[18] Accurate pure component spectra of $Rh_4(CO)_{12}$ and $Rh_6(CO)_{16}$ were readily recovered. For example, with the use of $z = 4$ right singular vectors, the entropies were 5.628 and 5.293, respectively.

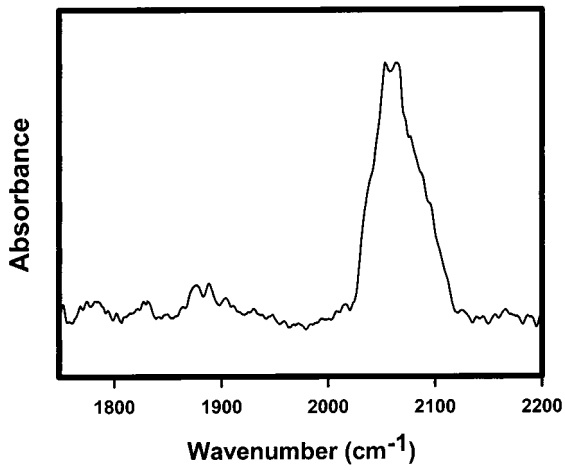

Figure 6. Estimated spectral pattern for suspended $Rh_6(CO)_{16}$ solids.

Reconstruction of the Spectra of Suspended $Rh_6(CO)_{16}$ Solid. Further inspection of the third and fourth vectors of the $\mathbf{V}^T$ matrix shows unusually broad and featureless absorbances in both the bridging and the terminal carbonyl regions. This is particularly apparent in the fourth right singular vector, where a corresponding maximum can be found at ca. 2053 cm^{-1} (indicated with a square in Figure 3). This feature was targeted as a local maximum at 2050−2060 cm^{-1}, with $z = 10$ vectors.[19] The result is shown in Figure 6. The resultant spectrum is due to the small amounts of suspended undissolved $Rh_6(CO)_{16}$ solid. Unfiltered solutions show a similar but stronger absorbance. The total integrated absorbance of the $Rh_6(CO)_{16}$ solid accounts for only 0.04% of the original experimental observations.

Discussion

Experimental Approximation and Signal Recovery. The primary strengths of the BTEM algorithm are (i) its computational efficiency, (ii) its ability to reconstruct an entire function (individual pure component spectrum) from a single targeted region, and (iii) its achievement of maximum signal recovery due to the use of a large number of singular vectors $z > s$. The first two issues were the emphasis of previous sections.

Concerning the last issue, a simple illustration is provided by considering the *overall* degree to which the preconditioned absorbance matrix $\mathbf{A}_{10\times2251}$ can be ap-

(18) *18.* $\alpha = 1.0$ is used in eq 20 for both the targeted regions 2069−2071 and 2075−2076 cm^{-1}.

(19) *19.* $\alpha = 1.0$ is used in eq 20 for the targeted region 2050−2060 cm^{-1}.

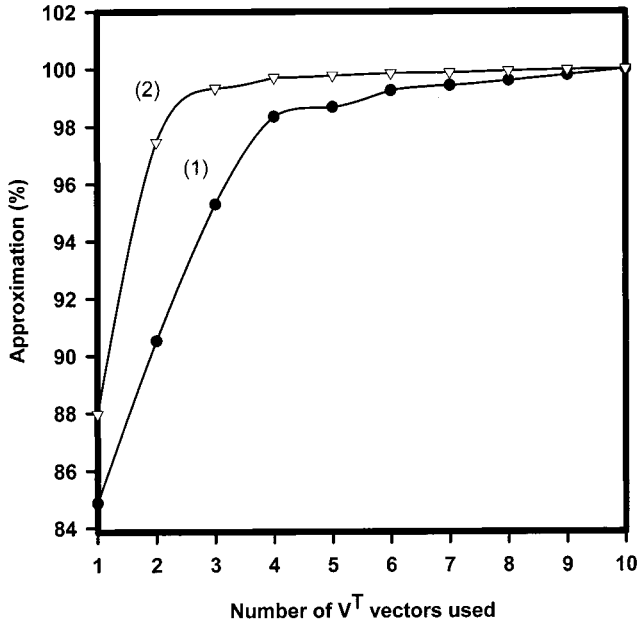

Figure 7. Degree of approximation for preconditioned absorbance matrix $\mathbf{A}_{10\times2251}$: (1) approximation based on eq 22; (2) approximation based on eq 23.

proximated, based on the number of right singular vectors used. This issue is related to, but is slightly different from, the *individual* estimates of $Rh_4(CO)_{12}$ and $Rh_6(CO)_{16}$ presented in Figures 4 and 5. Even though there are only two soluble species $Rh_4(CO)_{12}$/$Rh_6(CO)_{16}$ in the system, spectral features from these species are clearly identifiable in the third and fourth right singular vectors—and therefore the use of two right singular vectors is certainly insufficient.

The results of the calculations for overall signal recovery as a function of the number of right singular vectors (see Computational Aspects) can be seen in Figure 7. As expected, the use of only two right singular vectors accounts for only 90.5% of the experimental absorbance (or 97.5% of the variance). This is exceedingly low for a "simple" two-species system. However, the use of four right singular vectors accounts for a very respectable 98.4% of the experimental absorbance (99.7% of the variance). These four right singular vectors are the only vectors exhibiting pronounced localized spectral features. The use of more right singular vectors results in only minimal increment in the degree of approximation, and most of this can be attributed to randomly distributed instrumental and experimental error. Finally, since the individual reconstructed spectra obtained from the BTEM algorithm arise from the use of 4 or even 10 basis vectors, essentially all the usable chemically meaningful spectroscopic information from the data set is recovered.

Comparison of Results from BTEM and Other Spectral Reconstruction Methods. For comparison purposes, spectral reconstruction was also performed using other popular methods based on the self-modeling curve resolution (SMCR) technique, such as SIMPLISMA, IPCA, and OPA-ALS. The key concept used in both SIMPLISMA and IPCA is the computational identification of a "pure" wavelength for each component, followed by spectral reconstruction using least-squares approaches. IPCA obtains the pure wavelength

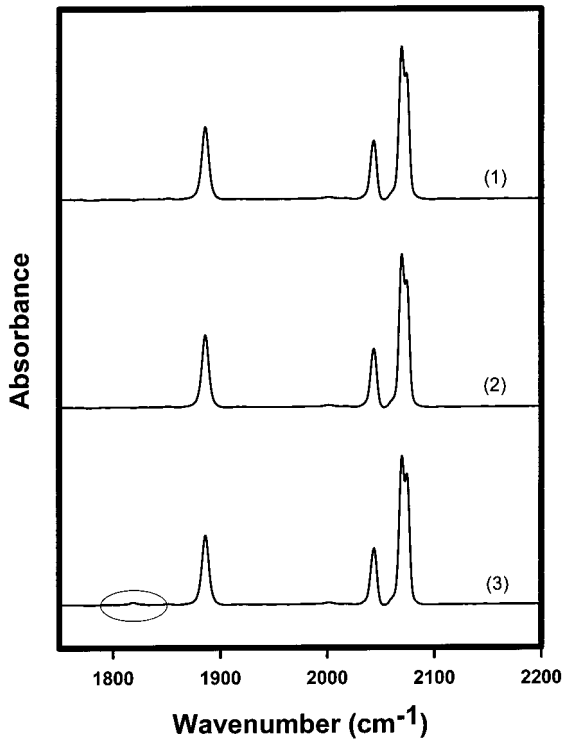

Figure 8. Estimated $Rh_4(CO)_{12}$ spectra via SIMPLISMA, IPCA, and OPA-ALS: (1) estimated spectrum via SIMPLISMA; (2) estimated spectrum via IPCA; (3) estimated spectrum via OPA-ALS.

by relying on principal component analysis, whereas SIMPLISMA does not. Different from the first two methods, OPA searches for the *s* (estimated number of pure components) most dissimilar spectra in the data and then uses an alternating least-squares (ALS) algorithm to improve the selected spectra via an iterative process.

The chosen degrees of freedom (number of components) for all three SMCR methods was $s = 3$. For SIMPLISMA, the noise level was set to 1.0% of the maximum mean signal. The IPCA algorithm was performed with SVD results of $\mathbf{A}_{10\times2251}$. For OPA-ALS, nonnegativity constraints on relative concentration and absorptivity were imposed, and the ALS code used was written by R. Tauler and A. de Juan.[20] These methods produced the pure component spectra estimates of $Rh_4(CO)_{12}$ and $Rh_6(CO)_{16}$ in solution and suspended undissolved $Rh_6(CO)_{16}$ solids shown in Figures 8−10, respectively.

For the reconstruction of $Rh_4(CO)_{12}$ shown in Figure 8, all three SMCR methods gave reasonable estimates. In addition, for the reconstruction of $Rh_6(CO)_{16}$, all three methods based on SMCR methods failed to produce results that are comparable with those from BTEM, as contributions from $Rh_4(CO)_{12}$ are clearly visible in the band at ca. 1886 cm^{-1}. Also, as seen in Figure 10, none of the SMCR methods were able to reconstruct the spectrum of suspended $Rh_6(CO)_{16}$ solids (note the minima at 2068 and 2073 cm^{-1} due to overcompensation of $Rh_4(CO)_{12}$ spectral signals). Furthermore, a second derivative based SIMPLISMA was performed and was found

(20) MATLAB code for ALS (als99.m), written by R. Tauler and A. de Juan, is available on the Internet. URL: http://www.ub.es/gesq/mcr/mcr.htm.

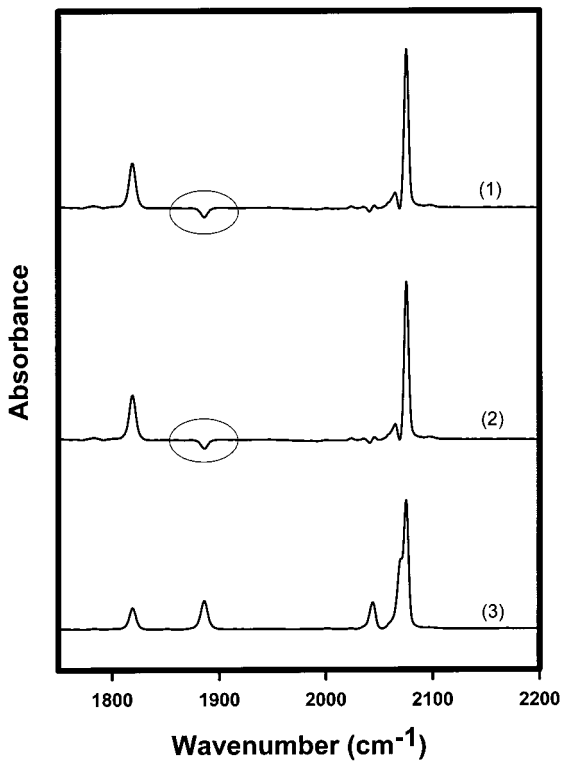

Figure 9. Estimated $Rh_6(CO)_{16}$ spectra via SIMPLISMA, IPCA, and OPA-ALS: (1) estimated spectrum via SIMPLISMA; (2) estimated spectrum via IPCA; (3) estimated spectrum via OPA-ALS.

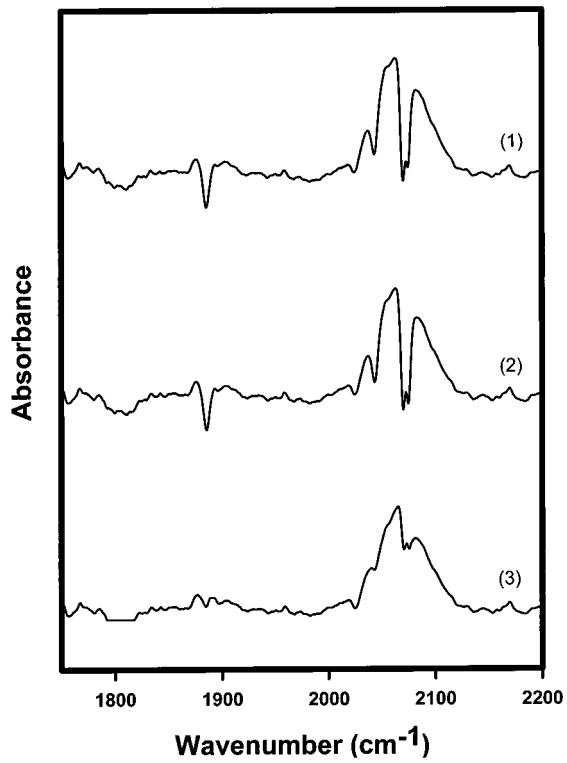

Figure 10. Estimated spectral pattern for suspended $Rh_6(CO)_{16}$ solids via SIMPLISMA, IPCA, and OPA-ALS: (1) estimated spectrum via SIMPLISMA; (2) estimated spectrum via IPCA; (3) estimated spectrum via OPA-ALS.

to fail completely for the present study, with results worse than those shown for SIMPLISMA in Figures 8−10.

Table 1. First-Derivative Entropy Values of Experimental and Estimated $Rh_4(CO)_{12}$ and $Rh_6(CO)_{16}$ Spectra

	$Rh_4(CO)_{12}$	$Rh_6(CO)_{16}$
preconditioned exptl spectrum	5.623	5.253
2 $\mathbf{V}^T$ vector BTEM est[a]	5.734	5.341
4 $\mathbf{V}^T$ vector BTEM est[a]	5.630	5.327
4 $\mathbf{V}^T$ vector BTEM est[b]	5.628	5.293
10 $\mathbf{V}^T$ vector BTEM est[a]	5.623	5.299
SIMPLISMA est	5.731	5.423
IPCA est	5.934	5.739
OPA-ALS est	5.744	5.745

[a] Estimated with spectral features in bridging carbonyl region. [b] Estimated with spectral features in terminal carbonyl region.

Table 1 summarizes the first spectral derivative based Shannon entropy values of the spectral estimates for $Rh_4(CO)_{12}$ and $Rh_6(CO)_{16}$. Clearly, the BTEM algorithm produces considerably more accurate and "simpler" spectral estimates than the other methods for these data. An alternate comparison of the spectral estimates using these different methods to the experimentally measured, but not pure, reference spectra for $Rh_4(CO)_{12}$ and $Rh_6(CO)_{16}$ (using for example an inner product) is not the appropriate way to compare results.

Conclusions

The newly developed band-target entropy minimization (BTEM) algorithm offers a number of significant improvements for spectral reconstruction. First and foremost, it offers a direct means of targeting the reconstruction of individual pure component spectra one at a time by a user-guided choice of priority spectral regions—even if these regions are highly overlapping. Second, it achieves a maximum degree of signal recovery due to the use of a large number of right singular vectors, $z > s$. Third, it is computationally more efficient than our previous algorithms in the sense that complexity (computational time) increases linearly with s. Although the results with a two-species unstable organometallic system $Rh_4(CO)_{12}$ and $Rh_6(CO)_{16}$ are extremely impressive—indeed BTEM outperformed SIMPLISMA, IPCA, OPA-ALS—*the real strength of the algorithm is clearly its applicability to very large sets of unknown species, such as those arising from in-situ spectroscopic studies of reactive systems.*[21] In such systems, many of the unknown components exist in trace amounts, and the signal intensities are very low. In the present tests, the BTEM algorithm was successful in recovering the pure component spectra of $Rh_4(CO)_{12}$, $Rh_6(CO)_{16}$ and $Rh_6(CO)_{16}$ solid, whose integrated absorbances account for only 0.3, 0.09, and 0.04% of the experimental data.

Experimental Section

Chemistry. As mentioned, the metal carbonyl cluster $Rh_4(CO)_{12}$ is thermally unstable and very sensitive to trace moisture and oxygen. Therefore, solution preparations of $Rh_4(CO)_{12}$ always show the presence of $Rh_6(CO)_{16}$. Additionally, if the solution is not maintained under a considerable CO partial pressure, further rapid degradation occurs. Accordingly, room-temperature "pure" $Rh_4(CO)_{12}$ infrared spectra, without a contribution from $Rh_6(CO)_{16}$, are impossible to obtain. The overall reaction can be written as

(21) Widjaja, E.; Li, C.; Garland, M. *Organometallics* **2002**, *21*, 1991.

$$6Rh_4(CO)_{12} \leftrightarrow 4Rh_6(CO)_{16} + 8CO \quad (4)$$

Mixture Preparation. Crystalline $Rh_4(CO)_{12}$ (98% min) and $Rh_6(CO)_{16}$ (99%+) were purchased from Strem Chemicals (Newburyport, MA) and used as received. The solvent *n*-hexane (Fluka, puriss, 99.6%+) was refluxed over Na/K under argon (Soxal, 99.999%). All solution preparations were made using standard Schlenk techniques.[22,23]

Pure $Rh_4(CO)_{12}$ and $Rh_6(CO)_{16}$ stock solutions were first prepared. Although $Rh_4(CO)_{12}$ has a reasonable solubility of ca. 1.5 g/L, $Rh_6(CO)_{16}$ is only sparingly soluble at 293 K. Therefore, most solutions of $Rh_6(CO)_{16}$ have a poor baseline in the mid-infrared region due to the suspension of undissolved $Rh_6(CO)_{16}$ particles. To overcome this problem, only a very small amount of $Rh_6(CO)_{16}$ (ca. 10 mg) was added to 100 mL of *n*-hexane and this was continuously stirred for 1.5 h under 1 atm of argon to ensure maximum dissolution. After the larger undissolved $Rh_6(CO)_{16}$ solid particles were allowed to settle, the supernatant was further filtered with PTFE syringe filters of pore size 0.2 μm to remove additional $Rh_6(CO)_{16}$ solid particles. The filtered supernatant was then used in subsequent mixture preparations with the pure $Rh_4(CO)_{12}$ stock solution. The resulting infrared spectra had good baselines.

A total of 10 different and very dilute mixture solutions were prepared by mixing varying amounts of pure $Rh_4(CO)_{12}$ and $Rh_6(CO)_{16}$ stock solutions in different ratios. The measured absorbance for the bridging carbonyl are tabulated in Table 2.

Spectroscopy. Both $Rh_4(CO)_{12}$ and $Rh_6(CO)_{16}$ possess bridging as well as terminal metal carbonyl vibrations. The bridging vibrations are centered at ca. 1818 and 1885 cm^{-1}, respectively, and the terminal vibrations occur in the region of ca. 1950−2100 cm^{-1}.[24]

Measurements were made on a Perkin-Elmer 2000 FTIR spectrometer equipped with a DTGS detector. A standard CaF_2 IR cell, with ca. 0.5 mm optical path length, was used for all measurements. The optical, sample, and detector chambers of the spectrometer were continually purged with N_2 (Soxal, 99.999%) at a flow rate of ca. 2 L/min. All spectra were recorded on the range of 1750−2200 cm^{-1} with a resolution of 4 cm^{-1}. Data acquisition was made at 0.2 cm^{-1} intervals. Therefore, a total of 2251 channels were analyzed.

A total of 14 spectra were taken in this study, namely (i) one background air containing moisture and CO_2 signals, (ii) one CaF_2 cell with *n*-hexane reference, (iii) two pure rhodium carbonyl cluster stock solutions, and (iv) the 10 mixture solutions.

Computational Aspects

Computation. All algorithms were implemented in MATLAB. Calculations were performed on a Pentium II IBM-compatible personal computer of 400 MHz processing speed with 384 MB of RAM on a Win98 operating system.

Spectral Preconditioning. Each experimental solution spectrum $\mathbf{A}^{exp}_{1\times\nu}$ was preconditioned by subtraction of (i) the background reference, $\mathbf{A}^{ref}_{bac}$, and (ii) CaF_2 cell with *n*-hexane reference, $\mathbf{A}^{ref}_{cell+hex}$, according to eq 5, where the coefficients x_i are scalar subtraction factors, and $\mathbf{A}^{ref_i}_{1\times\nu}$ refers to either $\mathbf{A}^{ref}_{bac}$ or $\mathbf{A}^{ref}_{cell+hex}$.

$$\mathbf{A}^{pre}_{1\times\nu} = \mathbf{A}^{exp}_{1\times\nu} - \sum_i x_i \mathbf{A}^{ref_i}_{1\times\nu} \quad (5)$$

Table 2. Estimated Absorbance of $Rh_4(CO)_{12}$ and $Rh_6(CO)_{16}$ in 10 Mixture Solutions

mixture no.	$Rh_6(CO)_{16}$ est abs ($\times 10^3$)[a]	$Rh_4(CO)_{12}$ est abs ($\times 10^2$)[b]
1	4.25	1.677
2	5.36	1.062
3	3.86	1.884
4	1.97	0.751
5	2.75	0.505
6	2.83	0.474
7	0.43	1.256
8	1.24	1.035
9	1.35	0.934
10	1.60	0.665

[a] Measured at ca. 1819 cm^{-1}. [b] Measured at ca. 1886 cm^{-1}.

Entropy minimization was the basis for determining the optimal values of each x_i. The discrete form of the Shannon entropy function[25] for any arbitrary spectrum forms the objective function (eq 6), and the golden section search was used for optimization of x_i values.[26] The entropy function was based on the first derivative of the resultant subtracted spectrum $\mathbf{A}^{subtract}_{1\times\nu}$ evaluated at each point $A^{subtract}_{\nu}$ (eq 7). The final spectrum after optimally subtracting $\mathbf{A}^{ref}_{bac}$ and $\mathbf{A}^{ref}_{cell+hex}$ is the desired preconditioned spectrum $\mathbf{A}^{pre}_{1\times\nu}$. The algorithm is robust and stable, and produces smooth preconditioned spectra with extremely good baselines.

$$\min g = -\sum_{\nu} h_\nu \ln h_\nu \quad (6)$$

where

$$h_\nu = \left| \frac{dA^{subtract}_{\nu}}{d\nu} \right| \quad (7)$$

Spectral Analysis. The consolidated matrix of preconditioned mixture absorbance data is denoted $\mathbf{A}_{k\times\nu}$, where k denotes the number of mixture spectra and ν is the number of data channels associated with the experimental FTIR wavenumber range and interval taken. For the present $Rh_4(CO)_{12}/Rh_6(CO)_{16}$ mixture system, $k = 10$ and $\nu = 2251$.

According to the Lambert−Beer−Bouger law, the matrix is a product of a concentration matrix $\mathbf{C}_{k\times s}$ (which incorporates the path length l) and absorptivity matrix $\mathbf{a}_{s\times\nu}$. This absorbance data matrix $\mathbf{A}_{k\times\nu}$ can be subjected to singular value decomposition (SVD) (eq 8),[27] to obtain its abstract ortho-

$$\mathbf{A}_{k\times\nu} = \mathbf{C}_{k\times s}\mathbf{a}_{s\times\nu} + \epsilon_{k\times\nu} = \mathbf{U}_{k\times k}\Sigma_{k\times\nu}\mathbf{V}^{T}_{\nu\times\nu} \quad (8)$$

normal matrixes $\mathbf{U}_{k\times k}$ and $\mathbf{V}^{T}_{\nu\times\nu}$ with its singular matrix $\Sigma_{k\times\nu}$. Furthermore, $\mathbf{A}_{k\times\nu}$ can be approximated by eq 9, where s is

$$\mathbf{A}_{k\times\nu} \approx \hat{\mathbf{C}}_{k\times s}\hat{\mathbf{a}}_{s\times\nu} = \mathbf{U}_{k\times s}\Sigma_{s\times z}\mathbf{T}^{-1}_{s\times z}\mathbf{T}_{s\times z}\mathbf{V}^{T}_{z\times\nu} \qquad k \geq z \geq s \quad (9)$$

the number of species recovered and z is the number of right singular vectors used for spectral reconstruction. Note that $\mathbf{T}^{-1}_{s\times z}$ is the generalized inverse for a rectangular matrix, $\hat{\mathbf{a}}_{s\times\nu}$ is the matrix of averaged pure component expectations for s species, $\hat{\mathbf{C}}_{k\times s}$ is its corresponding expectation for concentration calculated from eq 10, and $\epsilon_{k\times\nu}$ is a combination of experimental error and spectral nonlinearities.[28]

(22) Shriver, D. F.; Drezdzon, M. A. *The Manipulation of Air-Sensitive Compounds*; Wiley: New York, 1986.
(23) Safety issues include the toxicity of rhodium carbonyls, as well as the pyrophoric nature of Na/K alloy.
(24) (a) Beck, W.; Lottes, K. *Chem. Ber.* **1961**, *94*, 2578. (b) Bor, G.; Sbrignadello, G.; Noack, K. *Helv. Chim. Acta* **1975**, *58*, 815. (c) Chini, P. *J. Chem. Soc. D* **1967**, 440. (d) James, B. R.; Rempel, G. L.; Teo, W. K. *Inorg. Synth.* **1976**, *16*, 49.
(25) Shannon, C. E. *Bell Syst. Technol. J.* **1948**, *27*, 379.
(26) Reklaitis, G. V.; Ravindran, A.; Ragsdell, K. M. *Engineering Optimization: Methods and Applications*; Wiley: New York, 1983.
(27) Golub, G. H.; Van Loan, C. F. *Matrix Computations*; Johns Hopkins University Press: Baltimore, MD, 1996.
(28) Garland, M.; Visser, E.; Terwiesch, P.; Rippin, D. W. T. *Anal. Chim. Acta* **1997**, *351*, 337.

$$\hat{\mathbf{C}}_{k\times s} = \mathbf{U}_{k\times s}\Sigma_{s\times z}\mathbf{T}^{-1}_{s\times z} = \mathbf{A}_{k\times \nu}\hat{\mathbf{a}}^{\mathrm{T}}_{\nu\times s}(\hat{\mathbf{a}}_{s\times \nu}\hat{\mathbf{a}}^{\mathrm{T}}_{\nu\times s})^{-1} \quad (10)$$

Instead of solving all rows of the transformation matrix $\mathbf{T}^{-1}_{s\times z}$ at once, the BTEM algorithm solves the problem one transformation row at a time (see the following subsection for details) and, hence, one spectrum at a time. The expectation for each spectrum $\hat{\mathbf{a}}_{1\times \nu}$ is then given by eq 11, with corresponding expectation for concentration $\hat{\mathbf{C}}_{k\times 1}$ given by eq 12. For the present case of $Rh_4(CO)_{12}/Rh_6(CO)_{16}$ mixtures, $z = 2, 4, 10$ vectors were used.

$$\hat{\mathbf{a}}_{1\times \nu} = \mathbf{T}_{1\times z}\mathbf{V}^{\mathrm{T}}_{z\times \nu} \qquad z \geq s \quad (11)$$

$$\hat{\mathbf{C}}_{k\times 1} = \mathbf{A}_{k\times \nu}\hat{\mathbf{a}}^{\mathrm{T}}_{\nu\times 1}(\hat{\mathbf{a}}_{1\times \nu}\hat{\mathbf{a}}^{\mathrm{T}}_{\nu\times 1})^{-1} \quad (12)$$

The objective function for optimizing the elements of $\mathbf{T}_{1\times z}$ in the BTEM algorithm is shown in eq 13. The first term on the right-hand side is the Shannon entropy function based on a first derivative of the absorbance estimate $\hat{\mathbf{a}}_{1\times \nu}$ (eq 14). The second term is a penalty function (eq 15) for ensuring (i) that there are non-negativities in each pure component spectral estimate $\hat{\mathbf{a}}_{1\times \nu}$ and each estimated concentration $\hat{\mathbf{C}}_{k\times 1}$, and (ii) that a reasonable maximum spectral absorbance $\hat{\mathbf{a}}^{\max}_{1\times \nu}$ is obtained. Together with the penalty function are three sets of associated scalar parameters: (i) γ_a, γ_c, $\gamma_{\max}$ are penalty coefficients for constraints defined by eqs 18−20, (ii) $\lambda_1 = 10^{-3}$ and $\lambda_2 = 10^{-2}$ are the bounds for the absorptivity constraint defined in eq 18, and (iii) α defined in eq 20 sets the maximum absorbance, in relation to the target band peak absorbance $\hat{\mathbf{a}}^{\mathrm{target}}_{1\times \nu}$, which is normalized to be identically 1.0 (see following subsection).

$$\min G = -\sum_{\nu} h_\nu \ln h_\nu + P(\hat{\mathbf{a}}_{1\times \nu}, \hat{\mathbf{C}}_{k\times 1}, \hat{\mathbf{a}}^{\max}_{1\times \nu}) \quad (13)$$

where

$$h_\nu = \frac{\left|\frac{d\hat{a}_\nu}{d\nu}\right|}{\sum_{\nu}\left|\frac{d\hat{a}_\nu}{d\nu}\right|} \quad (14)$$

$$P(\hat{\mathbf{a}}_{1\times \nu}, \hat{\mathbf{C}}_{k\times 1}, \hat{\mathbf{a}}^{\max}_{1\times \nu}) = \gamma_a F_1(\hat{a}_\nu) + \gamma_c F_2(\hat{C}_k) + \gamma_{\max} \quad (15)$$

where

$$F_1(\hat{a}_\nu) = \sum_{\nu=1}^{2251}(\hat{a}_\nu)^2 \;\forall\; \hat{a}_\nu < 0 \quad (16)$$

$$F_2(\hat{C}_k) = \sum_{k=1}^{10}(\hat{C}_k)^2 \;\forall\; \hat{C}_k < 0 \quad (17)$$

$$\gamma_a = \begin{cases} 0 & F_1(\hat{a}_\nu) < \lambda_1 \\ 10 & \lambda_1 \leq F_1(\hat{a}_\nu) < \lambda_2 \\ 10^4 & F_1(\hat{a}_\nu) \geq \lambda_2 \end{cases} \quad (18)$$

$$\gamma_c = 10^3 \;\forall\; F_2(\hat{C}_k) \quad (19)$$

$$\gamma_{\max} = \begin{cases} 10^4 & \hat{\mathbf{a}}^{\max}_{1\times \nu} > \alpha \\ 0 & \hat{\mathbf{a}}^{\max}_{1\times \nu} \leq \alpha \end{cases} \quad (20)$$

Band-Target Entropy Minimization (BTEM) Algorithm. In this new method, the vectors in the $\mathbf{V}^{\mathrm{T}}$ matrix were first inspected for significant spectral features. Such features usually appear only in the first few vectors of $\mathbf{V}^{\mathrm{T}}$, as they represent most of the variance in the preconditioned data matrix $\mathbf{A}_{k\times \nu}$. Since BTEM targets these features one at a time, narrow intervals corresponding to these local extrema are assigned.

For example, the characteristic bridging carbonyl band for $Rh_4(CO)_{12}$ occurs at ca. 1886 cm^{-1}. Therefore, upon visual inspection, clearly identifiable spectral features/extrema can be seen at ca. 1886 cm^{-1} in the initial three $\mathbf{V}^{\mathrm{T}}$ vectors. Accordingly, one sets the BTEM algorithm to target the interval 1885−1887 cm^{-1}. The algorithm then reconstructs the simplest function associated with this spectral feature such that the constraints imposed by eqs 13−20 are met.

The reason for taking a region of wavenumber for the targeted band rather than an exact singular band peak wavenumber is that *nonlinearities* due to band shifting and shape changes exist in real spectra. In the process of transforming the right singular vectors, the targeted band peak absorbance $\hat{\mathbf{a}}^{\mathrm{target}}_{1\times \nu}$ is normalized to 1.0, and the maximum of the estimated spectrum $\hat{\mathbf{a}}^{\max}_{1\times \nu}$ is constrained to be equal or less than the preassigned scalar value $\alpha \geq 1.0$ (eq 20). It is worth reiterating that no *a priori* information as such is required by this BTEM approach; only visual inspection of the right singular vectors.

Corana's Simulated Annealing. Corana's simulated annealing algorithm was employed to perform the global optimizations of the highly nonlinear BTEM objective function. Corana's simulated annealing is a random optimization method, modified from the original simulated annealing algorithm,[29] with dynamic step size generation and strict convergence criterion enhancements.[30] This algorithm has been extensively used and has proven capable of obtaining global solutions for highly nonlinear optimization problems.[31] A key feature of Corana's algorithm is its ability to escape local minima. This feature is based on the Metropolis selection criteria.

Overall Signal Recovery. Equation 21 can be solved for $z = 1, 2, \ldots, 10$ to successively approximate the preconditioned spectral absorbance matrix $\mathbf{A}_{10\times 2251}$. Furthermore, these approximations $\hat{\mathbf{A}}^{z}_{10\times 2251}$ can be compared to the real experimental absorbance matrix $\mathbf{A}_{10\times 2251}$ using eq 22 or in terms of the variance (eq 23). These degrees of approximation are expressed as a percentage.

$$\hat{\mathbf{A}}^{z}_{10\times 2251} = \mathbf{U}_{10\times z}\Sigma_{z\times z}\mathbf{V}^{\mathrm{T}}_{z\times 2251} \quad (21)$$

$$\text{approximation (\%)} = \left(1 - \frac{\sum_{k=1}^{10}\sum_{\nu=1}^{2251}||\mathbf{A}_{10\times 2251}| - |\hat{\mathbf{A}}^{z}_{10\times 2251}||}{\sum_{k=1}^{10}\sum_{\nu=1}^{2251}|\mathbf{A}_{10\times 2251}|}\right)\times 100 \quad (22)$$

$$\text{variance (\%)} = \left(1 - \frac{\sum_{k=1}^{10}\sum_{\nu=1}^{2251}|(\mathbf{A}_{10\times 2251})^2 - (\hat{\mathbf{A}}^{z}_{10\times 2251})^2|}{\sum_{k=1}^{10}\sum_{\nu=1}^{2251}(\mathbf{A}_{10\times 2251})^2}\right)\times 100 \quad (23)$$

OM0108752

(29) Kirkpatrick, S.; Gelatt, C., Jr.; Vecchi, M. *Science* **1983**, *220*, 671.

(30) Corana, A.; Marchesi, M.; Martini, C.; Ridella, S. *ACM Trans. Math. Software* **1987**, *13*, 263.

(31) (a) Goffe, W. L.; Ferrier, G. D.; Rogers, J. *J. Econometrics* **1994**, *60*, 65. (b) Asprey, S. P.; Batres, R.; Fuchino, T.; Naka, Y. *Ind. Eng. Chem. Res.* **1999**, *38*, 2364. (c) Asprey, S. P.; Naka, Y. *J. Chem. Eng. Jpn.* **1999**, *32*, 328.